Published in final edited form as:
Nat Med. 2009 October ; 15(10): 1219–1223. doi:10.1038/nm.1971.

Three-dimensional microscopy of the tumor microenvironment *in vivo* using optical frequency domain imaging

Benjamin J Vakoc[1,2,3,*], **Ryan M Lanning**[3,4,*], **James A Tyrrell**[4], **Timothy P Padera**[4], **Lisa A Bartlett**[1], **Triantafyllos Stylianopoulos**[4], **Lance L Munn**[4], **Guillermo J Tearney**[1,3,5], **Dai Fukumura**[4], **Rakesh K Jain**[4,†], and **Brett E Bouma**[1,†,2,3]

[1] Wellman Center for Photomedicine, 55 Fruit St., Boston, Massachusetts 02114, USA

[2] Department of Dermatology, Harvard Medical School and Massachusetts General Hospital, Boston, Massachusetts 02114, USA

[5] Department of Pathology, Harvard Medical School and Massachusetts General Hospital, Boston, Massachusetts 02114, USA

[3] Harvard-Massachusetts Institute of Technology Division of Health Sciences and Technology, 77 Massachusetts Avenue, E25-519, Cambridge, Massachusetts 02139, USA

[4] Edwin L. Steele Laboratory, Department of Radiation Oncology, Massachusetts General Hospital and Harvard Medical School, 100 Blossom Street, Boston, Massachusetts 02114, USA

Abstract

Intravital multiphoton microscopy has provided powerful mechanistic insights into health and disease, and has become a common instrument in the modern biological laboratory. The requisite high numerical aperture and exogenous contrast agents that enable multiphoton microscopy, however, limit ability to investigate substantial tissue volumes or to probe dynamic changes repeatedly over prolonged periods. Here, we introduce optical frequency domain imaging (OFDI) as an intravital microscopy that circumvents the technical limitations of multiphoton microscopy and, as a result, provides unprecedented access to previously unexplored, critically important aspects of tissue biology. Using novel OFDI-based approaches and entirely intrinsic mechanisms of contrast, we present rapid and repeated measurements of tumor angiogenesis, lymphangiogenesis, tissue viability and both vascular and cellular responses to therapy, thereby demonstrating the potential of OFDI to facilitate the exploration of physiological and pathological processes and the evaluation of treatment strategies.

†Authors to whom correspondence should be addressed: R.K.J (jain@steele.mgh.harvard.edu) or B.E.B (bouma@helix.mgh.harvard.edu).
*Authors contributed equally to this work

Author Contributions

BJV developed OFDI technology, designed and performed most of the experiments, developed methodology, headed all data analysis and wrote the manuscript. RML designed and performed most of the experiments, developed methodology, headed all data analysis and wrote the manuscript. JAT contributed to vascular tracing of OFDI data. TPP performed lymphangiography experiments and contributed to data analysis and manuscript preparation. LAB performed VEGF-R2 blockade *in vivo* experiments. TS developed and performed fractal characterization and contributed to manuscript preparation. LLM contributed to vascular data analysis. GJT contributed to OFDI technology development. DF contributed to experimental design and manuscript preparation. RKJ and BEB contributed to the design of experiments, preparation of the manuscript, and supervised the project.

Introduction

The application of multiphoton microscopy[1,2] (MPM) to the study of solid tumor biology *in vivo* has elucidated pathways and mechanisms of cancer progression and has led to new therapeutic strategies[3]. Current high-resolution intravital imaging techniques, however, permit visualization of tumor microstructure and vascular morphology only superficially (300–400 μm depth) and only over volumetric regions that are a fraction of the total tumor volume in small animal models. Additionally, longitudinal imaging is often limited in frequency due to the accumulation of exogenous contrast agents. Consequently, nearly a decade after the introduction of MPM to tumor biology, significant gaps remain in our understanding of the vascularization of tumors, the multifaceted interactions between tissues and vessels within the heterogeneous tumor mass, and the response of blood vessels, lymphatic vessels and cancer cells to therapy. New methods that complement existing MPM techniques by probing the tumor microenvironment over wider fields and broader timescales are needed to fill these gaps.

Optical coherence tomography[4] (OCT) is an alternative approach for *in vivo* microscopy that supports imaging at these expanded spatiotemporal scales. However, methods for effectively characterizing biological parameters of the tumor microenvironment and structure are lacking in OCT and existing angiographic OCT systems have not achieved the high sensitivity and the rapid imaging speeds required for large-volume vascular morphometry. Here, we overcome these limitations by developing new methods and instrumentation for a second generation OCT technology termed optical frequency domain imaging (OFDI)[5]. We apply these techniques to a range of tumor models *in vivo* and demonstrate the ability of OFDI to perform 1) high-resolution, wide-field, and deep imaging of tumor vasculature, 2) morphological and fractal characterization of vascular networks, 3) contrast-free functional lymphangiography and 4) characterization of tissue viability. Further, we demonstrate the application of these capabilities to reveal the responses of tumors *in vivo* to vascular-targeted and cellular-targeted therapies.

Results

We characterized the microenvironment of multiple tumor models at varying sites in mice using OFDI. The imaging system (Supplementary Fig. 1 online) was developed in-house and scanned a focused laser beam onto the tissue sample while recording the reflected optical signals. Cross-sectional images were provided in real-time and postprocessing was used to provide three-dimensional perspectives and quantitative analysis of biological parameters (Fig. 1a, Supplementary Fig. 2 online).

Wide-field three-dimensional angiography

The microvasculature of solid tumors plays a critical role in both progression and response to therapy[6]. To detect vessels in OCT, contrast is derived from the Doppler shift[7–12] induced by circulating red blood cells. Using novel implementations of Doppler principles and OFDI[13], we enabled wide-field angiography with sufficient speed to perform imaging over wide-fields and sensitivity to map smaller vessels, specificity to discriminate vascular motion from physiological motion (Supplementary Methods online). Three-dimensional angiographic datasets were derived from the acquired OFDI signals and were reduced to *en face* vascular projections using color to encode depth (Fig. 1b). Vascular projections were obtained across multiple tumor types at various sites (Supplementary Figs. 3 and 4 online), and additionally in normal tissues including the mammary fat pad and marrow space within the calvarium (Supplementary Fig. 5 online).

To provide gross perspective of the relative merits and complementary nature of Doppler OFDI and MPM angiography, tumors were imaged sequentially with each modality (Fig. 2, Supplementary Methods online). Whereas MPM excelled at visualizing the smallest superficial

capillaries (Fig. 2e,f), Doppler OFDI was superior in discerning vessels deeper within the central regions of the tumor and in regions where fluorescent tracers extravasated (Fig. 2c,d). Vessels beyond 1.0 mm in depth were routinely observed with Doppler OFDI while with MPM the maximum penetration depth in the surveyed tumor models ranged from 250 to 400 μm. The unique Doppler acquisition techniques incorporated into the OFDI instrument allowed rapid visualization of the tumor vasculature inclusive of its connectivity with host vessels, complementing the higher resolution but relatively superficial angiography provided by MPM.

Morphological and fractal characterization of vascular networks

Morphological characterization of blood vessels in tumors provides insight into resistance to transport, angiogenic mechanisms, and response to therapy[14,15]. Previous characterization methods, based on intravital microscopy and MPM angiography, however, have been limited to small fields-of-view and superficial depths. To extract quantitative vascular measurements from the OFDI angiograms, we developed a fully automated three-dimensional vascular tracing and analysis algorithm, optimized specifically to operate on the OFDI datasets (Supplementary Methods online). The algorithm reduced three-dimensional OFDI angiograms to networks of interconnected vessel segments modeled as superellipsoids[16]. From the centerlines and shape parameters of these superellipsoids, the trajectories and morphology of vessel segments were extracted (Supplementary Fig. 6). A comparison of co-registered vessel segment diameters derived from MPM and OFDI angiograms (Fig. 2g,h) indicated a high correlation ($r = 0.87$) for vessels measuring larger than 12 μm in diameter by MPM (Fig. 2i). For capillaries smaller than 12 μm in diameter, OFDI methods often located and traced the vessel segments but overestimated diameters, resulting in a lower correlation ($r = 0.36$).

The ability of OFDI to extract vascular parameters over larger volumes presents new opportunities for network characterization. Fractal analysis has been invoked to quantify the ability of a vascular network to provide an efficient transport of blood-borne nutrients, oxygen, or drugs within the tumor[14]. The fractal dimension is a statistical measure indicating how completely a network fills space. In three-dimensional geometries, an optimal space-filling network has a fractal dimension of three; lower fractal dimensions indicate a lesser degree of space filling. Using the topology and branching patterns derived from the OFDI datasets, we have analyzed the three-dimensional fractal dimension of tumor vasculature *in vivo* (Supplementary Methods online). An analysis of the vascular network depicted in Fig. 1b yielded a fractal dimension of 2.74 in the tumor region in agreement with results expected from prior two-dimensional analyses, and 3.02 in a normal region of the right hemisphere consistent with a fully developed capillary network filling three-dimensional space[17,18] (Supplementary Fig. 7 online).

Lymphangiography

Lymphangiography is typically performed by injecting a visible or fluorescent dye and imaging uptake and drainage via the lymphatic vessels. This approach, however, obscures structures near the site of injection and highlights only those lymphatic vessels draining the region of the injection. In OFDI, lymphatic networks appear as structures with negligible scattering intensity. The reduced scattering of the lymph relative to surrounding tissue is likely associated with its hypocellularity (Fig. 3a). Using these scattering characteristics, lymphatic vessels were identified, mapped, and segmented in the OFDI datasets (Supplementary Methods online). OFDI images of lymphatic networks in normal mouse skin showed functional lymphatic vessels highlighted with conventional Evan's blue lymphangiography, as well as additional vessels draining other regions of the skin (Fig. 3b,c). Enlarged peritumoral lymphatics were observed for human sarcoma (HSTS) models growing in the dorsal skinfold of mice (81 ± 4 μm; <2mm from tumor versus 40 ± 3 μm; >2mm from tumor: $P < 0.05$), consistent with previous measurements[19,20] (Fig. 3d). OFDI cross-sectional images were helpful in identifying

cellular masses within the lymphatics (Fig. 3e). By eliminating the need for exogenous contrast agents, OFDI allowed the monitoring of functional lymphatic vessels throughout tumor progression (Supplementary Fig. 8 online). Importantly, OFDI lymphangiography can be performed simultaneously with OFDI angiography (Supplementary Fig. 3 online); the two techniques differ only in the methods for postprocessing of the OFDI data.

Imaging tissue viability

Cell-targeted therapies are traditionally studied through assessment of tumor growth delay and histological examinations. These techniques, however, have their inherent limitations. Through the dependence of tissue scattering on cellular structures[21], it is possible to differentiate necrotic/apoptotic regions within a tumor from viable regions in three-dimensions using OFDI. Higher scattering regions within a murine mammary carcinoma (MCaIV) were found to be spatially co-registered with necrotic/apoptotic regions defined by corresponding hematoxylin and eosin staining (Fig. 4a). These regions were observed to expand, encompassing an increasing fraction of tumor volume during tumor progression (Fig. 4b,c).

Multiparametric monitoring of therapeutic response

To demonstrate OFDI's capacity to reveal the tumor response to therapy, we monitored changes induced by vascular or cellular targeted therapy. In the first set of experiments, mice with MCaIV tumors were imaged every other day up to 9 days during treatment with vascular endothelial growth factor receptor-2 (VEGFR-2) blocking monoclonal antibody DC101. Control animals had the same tumor preparation but received non-specific rat IgG. We imaged every two days post-implantation and defined starting points for each animal based on the status of the vascular network and the tumor volume. OFDI measurements of pre-treatment and control mean vessel diameters in 11 total tumors were consistent with previously published results using MPM[22] (55.8 ± 3.4 μm versus 49.8 ± 5.1 μm respectively). OFDI angiograms, acquired at day 5, consistently demonstrated a more dense and chaotic vascular network in the control group relative to the treated group (Fig. 5a). We found a reduction in both mean intratumor vessel length ($P = 0.001$) and diameter ($P = 0.029$) with DC101 treatment, consistent with findings of the previous study[22] (Fig. 5b). At day 7, the mean tumor volume within the treated group was 25% of that in the control group (Fig. 5b). Geometrical properties of the tumor vascular network showed a less pronounced response between groups. The fractal dimensions of both treatment and control groups reached plateaus (2.54 ± 0.04 and 2.60 ± 0.01, respectively) at day 3, and the mean tortuosity (see Supplementary Methods online) in the treated group was slightly lower than that of the control group at the conclusion of the study (Fig. 5b).

To observe short timescale vascular dynamics induced by anti-angiogenic therapy, we imaged MCaIV tumors growing in the dorsal skinfold chamber every 4 hours for 48 hours. We administered either DC101 or non-specific rat-IgG immediately after the initial imaging session. Promptly following VEGFR-2 blockade, the mean vessel diameter began to decrease while the tumor volume continued to expand. These trends continued throughout the 48-hour time course of the study (Supplementary Fig. 9 online). Time-lapse images of vascular responses acquired every 2 h for 48 h highlight the unprecedented ability of OFDI to monitor vascular dynamics over wide fields (Supplementary Video 1 online).

In the second set of experiments, we applied OFDI to investigate direct targeting of tumor cells. Diphtheria toxin accumulates in human cells, halting protein synthesis and eventually inducing apoptosis, but does not affect murine cells[23,24]. Therefore, in mouse xenograft models, diphtheria toxin can be used to model a cytotoxic treatment that is not confounded by direct damage to vascular endothelial cells. When we administered diphtheria toxin into mice bearing a human colorectal adenocarcinoma xenograft (LS174T) grown in the dorsal skin chamber,

apoptosis was evident within two days through associated changes in tumor scattering properties (Fig. 5c). During the first 24 h, the tumor volume remained approximately constant (Fig. 5d). After 24 h, widespread necrotic/apoptotic regions were observed within the volume of the treated tumors and the mean tumor volume began to decrease rapidly. After 48 h, the intratumor vessel length rapidly decreased, presumably due to the down-regulation or depletion of tumor cell-derived angiogenic growth factors (Fig. 5d).

Discussion

Through the development of novel techniques, instrumentation and algorithms, we have demonstrated the unique capabilities of OFDI to image the microenvironment of tumors *in vivo* rapidly and persistently over time without requiring exogenous contrast agents. These capabilities provide a new tool to probe the dynamics of tumor growth and response to therapy over substantially more of the tumor volume than can be accessed by higher resolution approaches such as MPM. As such, OFDI bridges a gap between subcellular resolution optical microscopies and alternative techniques, such as Doppler ultrasonography, magnetic resonance imaging, and micro-computed tomography (CT), which can penetrate deeper into tissue but that are limited to resolutions above ~50 μm.

Our results show frequent angiographic imaging over extended periods in the context of therapeutic intervention is possible using OFDI. Further, the ability to perform tracer-free lymphangiography of functional lymphatic networks with OFDI is a critical advance in the field that allows dynamic monitoring of the lymphatic vasculature during cancer progression and lymphedema[20,25]. The unique capability of OFDI to longitudinally image tissue viability and to spatially co-register this information with tumor vasculature opens new possibilities for the evaluation of existing therapeutic approaches and the rational design of therapeutic regimens. In concert, these capabilities present a powerful tool that complements and is likely to become as widely used as MPM in the study of solid tumors and the screening and development of vascular targeted and cellular targeted agents in cancer therapy.

Methods

OFDI system, signal and image processing, and quantitative analysis

OFDI provides high resolution imaging of the elastic light scattering properties of a sample in three dimensions[5]. Beam focusing provides transverse (x,y) discrimination of signals. Interferometric measurements of optical delay gate signals across the axial (z) dimension. The measurements first sample in parallel the interference signal between light scattered at all detectable depths and an external reference beam as a function of wavelength. Subsequent Fourier analysis of this interference signal across wavelength separates the combined signals across all depths into a depth-resolved scattering profile. The construction and design of the OFDI system (Supplementary Fig. 1 online) and the algorithms used to derive images from the OFDI dataset and extract quantitative data are described in the Supplementary Methods.

Animal models

Dorsal skinfold chambers and mammary fat pad windows were prepared in SCID mice as previously described[26–28]. The appropriate tumor type was then implanted in the center of the chamber 2–3 d after the initial surgery. The murine mammary adenocarcinoma (MCaIV), human colorectal adenocarcinoma (LS174T), and human soft tissue sarcoma (HSTS26T) were transplanted from subcutaneous tumors grown in isogenic mice. The human mammary adenocarcinoma (MDA-MB-361HK) was implanted as a single cell suspension of ~3×10^6 cells in 30 μl of Hank's Buffered Salt Solution (HBSS). Cranial windows were prepared in nude mice as previously described[28] and either human glioblastoma multiforme (U87) tumor tissue

was implanted 400 microns deep in the posterior cortex or MCaIV tissue was implanted in the leptomeninges of the left hemisphere. Tumors were generally allowed to grow for 2 weeks to a size of 4 mm in diameter by en face measurement depending on experimental protocol. Animals were anesthetized using either Ketamine/Xylene(10/1 mg ml^{-1}) or Isoflurane (1% in 100% oxygen), as indicated for each specific experiment. All animal work was approved by the by the MGH Institutional Animal Care and Use Committee.

Anti-angiogenic therapy: VEGF-R2 blockade

DC101 (ImClone Systems Inc.) or nonspecific rat IgG were administered intraperitoneally at 40mg/kg as prescribed in previous studies[22]. Mice were imaged every 2 d beginning 5 or 6 d after tumor implantation. Therapeutic initiation was determined through monitoring of tumor growth by both visual inspection and OFDI angiography. Animals were selected for the study based on the criteria that 1) the maximum tumor diameter was approximately 4 mm in diameter by en face measurement 2) the entire margin of the tumor was functionally vascularized and 3) the animal was in good health. Treatment group assignment was made randomly and masked during the duration of therapy to remove bias. Three treatments at three-day intervals were given (defined as day 0, 3, 6), and imaging was performed through day 9. Tumor growth delay was calculated from measurements of tumor volume by OFDI microanatomy measurements.

Cytotoxic therapy

Diphtheria toxin (Sigma-Aldrich Co.) was administered intraperitoneally at 30 μg kg^{-1} as previously described[24]. For control animals, a similar volume of saline was injected intraperitoneally. Male SCID mice bearing human colorectal adenocarcinoma tumors in the DSC were treated once and monitored over 10 d. During the initial 24 h, OFDI multiparametric measurements were made every 12 h followed by measurements every other day as described in the Supplementary Methods.

Prolonged time-lapse imaging

Imaging was performed under gas anesthesia (1% Isoflurane in oxygen) every 4 h for 48 total hours in mice bearing MCaIV mouse mammary carcinoma tumors in the DSC. Each imaging session was 5–10 m in duration, between which the experimental animal was returned to its cage. DC101 or non-specific Rat IgG (40 mg kg^{-1} i.p.) was administered once after the first imaging session. To generate the shorter interval time-lapse video, a separate SCID mouse bearing MCaIV in the DSC was imaged every 2 h for 48 total hours. DC101 was administered (40 mg kg^{-1} i.p.) once 8 h after the first imaging session. The resulting angiographic images for each time point were manually cropped and aligned using Adobe Photoshop (Adobe Systems Inc.) and ImageJ to generate the time-lapse video.

Evan's Blue Lymphangiography

Lymphangiography was performed by injecting 10 μl of 4% Evan's Blue into the tissue and observing nearby lymphatic vessels with a dissecting scope.

Statistical analysis

Statistical analysis. Data are presented as mean ± standard error of the mean (SEM). Significant differences between groups were determined by a multivariate repeated measures ANOVA accounting for response to treatment over time (Systat, Systat Software, Inc.). For quantitative metrics calculated by the vascular tracing algorithm, such as vascular diameters, significant differences at each time-point were determined by a two-sample Student's t-test. For tumor growth, statistical differences at each time-point were determined by the non-parametric Mann-Whitney test. Statistical differences at given time-points are denoted on the plots by asterisks. p-value ≤ 0.05 was considered statistically significant for all comparisons. The multiphoton

and OFDI measurements of vessel diameters (Fig. 2i) were compared using the Pearson product-moment correlation.

Supplementary Material

Refer to Web version on PubMed Central for supplementary material.

Acknowledgments

We thank J. Baish, for insightful input regarding fractal analysis. We also thank J. Kahn and S. Roberge for preparation of animal models, P. Huang, for animal care and colony maintenance, and E. di Tomaso. and C. Smith for histological preparations. We thank Genentech for supplying the MDA-MB-361HK mammary carcinoma cells, and Dr. John B. Little of the Harvard School for Public Health for HSTS26T. This research was funded in part by US National Institute of Health grants P01-CA80124, R01-CA85140, R01 CA126642, R33-CA125560, K25-CA127465, K99-CA137167, R01-CA96915, and R01-CA115767. RML is supported in part by US Department of Defense Breast Cancer Research Program fellowship W81XWH-06-1-0436.

References

1. Masters, BR.; So, PT. Handbook of Biomedical Nonlinear Optical Microscopy. Oxford University Press; New York: 2008.
2. Brown EB, et al. In vivo measurement of gene expression, angiogenesis and physiological function in tumors using multiphoton laser scanning microscopy. Nat Med 2001;7:864–868. [PubMed: 11433354]
3. Jain RK. Normalization of tumor vasculature: An emerging concept in antiangiogenic therapy. Science 2005:58–62. [PubMed: 15637262]
4. Huang D, et al. Optical coherence tomography. Science 1991;254:1178. [PubMed: 1957169]
5. Yun SH, Tearney GJ, de Boer JF, Iftimia N, Bouma BE. High-speed optical frequency-domain imaging. Opt Express 2003;11:2953–2963. [PubMed: 19471415]
6. Carmeliet P. Angiogenesis in life, disease and medicine. Nature 2005;438:932–936. [PubMed: 16355210]
7. Izatt JA, Kulkami MD, Yazdanfar S, Barton JK, Welch AJ. In vivo bidirectional color Doppler flow imaging of picoliter blood volumes using optical coherence tomograghy. Opt Lett 1997;22:1439–1441. [PubMed: 18188263]
8. Chen ZP, Milner TE, Dave D, Nelson JS. Optical Doppler tomographic imaging of fluid flow velocity in highly scattering media. Opt Lett 1997;22:64–66. [PubMed: 18183104]
9. Zhao Y, et al. Phase-resolved optical coherence tomography and optical Doppler tomography for imaging blood flow in human skin with fast scanning speed and high velocity sensitivity. Opt Lett 2000;25:114–116. [PubMed: 18059800]
10. Vakoc BJ, Yun SH, de Boer JF, Tearney GJ, Bouma BE. Phase-resolved optical frequency domain imaging. Opt Express 2005;13:5483–5493. [PubMed: 19498543]
11. Collins HA, et al. Blood-vessel closure using photosensitizers engineered for two-photon excitation. Nat Photonics 2008;2:420–424.
12. Wang RKK, Hurst S. Mapping of cerebro-vascular blood perfusion in mice with skin and skull intact by optical micro-angiography at 1.3 mu m wavelength. Opt Express 2007;15:11402–11412. [PubMed: 19547498]
13. Yun SH, et al. Comprehensive volumetric optical microscopy in vivo. Nat Med 2006;12:1429–1433. [PubMed: 17115049]
14. Baish JW, Jain RK. Fractals and Cancer. Cancer Res 2000;60:3683–3688. [PubMed: 10919633]
15. Jain RK. Molecular regulation of vessel maturation. Nat Med 2003;9:685–693. [PubMed: 12778167]
16. Tyrrell JA, et al. Robust 3-D modeling of vasculature imagery using superellipsoids. IEEE Trans Med Imaging 2007;26:223–237. [PubMed: 17304736]
17. Gazit Y, et al. Fractal characteristics of tumor vascular architecture during tumor growth and regression. Microcirculation 1997;4:395–402. [PubMed: 9431507]

18. Gazit Y, Berk DA, Leunig M, Baxter LT, Jain RK. Scale-Invariant Behavior and Vascular Network Formation in Normal and Tumor Tissue. Phys Rev Lett 1995;75:2428–2431. [PubMed: 10059301]

19. Isaka N, Padera TP, Hagendoorn J, Fukumura D, Jain RK. Peritumor lymphatics induced by vascular endothelial growth factor-C exhibit abnormal function. Cancer Res 2004;64:4400–4404. [PubMed: 15231646]

20. Padera TP, et al. Lymphatic metastasis in the absence of functional intratumor lymphatics. Science 2002;296:1883–1886. [PubMed: 11976409]

21. Sharma M, Verma Y, Rao KD, Nair R, Gupta PK. Imaging growth dynamics of tumour spheroids using optical coherence tomography. Biotechnol Lett 2007;29:273–278. [PubMed: 17160349]

22. Tong RT, et al. Vascular normalization by vascular endothelial growth factor receptor 2 blockade induces a pressure gradient across the vasculature and improves drug penetration in tumors. Cancer Res 2004;64:3731–3736. [PubMed: 15172975]

23. Arbiser JL, et al. Isolation of mouse stromal cells associated with a human tumor using differential diphtheria toxin sensitivity. Am J Pathol 1999;155:723–729. [PubMed: 10487830]

24. Padera TP, et al. Cancer cells compress intratumour vessels. Nature 2004;427:695. [PubMed: 14973470]

25. Padera TP, et al. Differential response of primary tumor versus lymphatic metastasis to VEGFR-2 and VEGFR-3 kinase inhibitors cediranib and vandetanib. Mol Cancer Ther 2008;7:2272–2279. [PubMed: 18687659]

26. Jain, RK.; Brown, EB.; Munn, LL.; Fukumura, D. Intravital microscopy of normal and diseased tissues in the mouse. In: Goldman, RD.; Spector, DL., editors. Live cell imaging: a laboratory manual. Cold Spring Harbor Laboratory Press; Cold Spring Harbor, N.Y: 2005. p. 435-466.

27. Leunig M, et al. Angiogenesis, microvascular architecture, microhemodynamics, and interstitial fluid pressure during early growth of human adenocarcinoma LS174T in SCID mice. Cancer Res 1992;52:6553–6560. [PubMed: 1384965]

28. Yuan F, et al. Vascular permeability and microcirculation of gliomas and mammary carcinomas transplanted in rat and mouse cranial windows. Cancer Res 1994;54:4564–4568. [PubMed: 8062241]

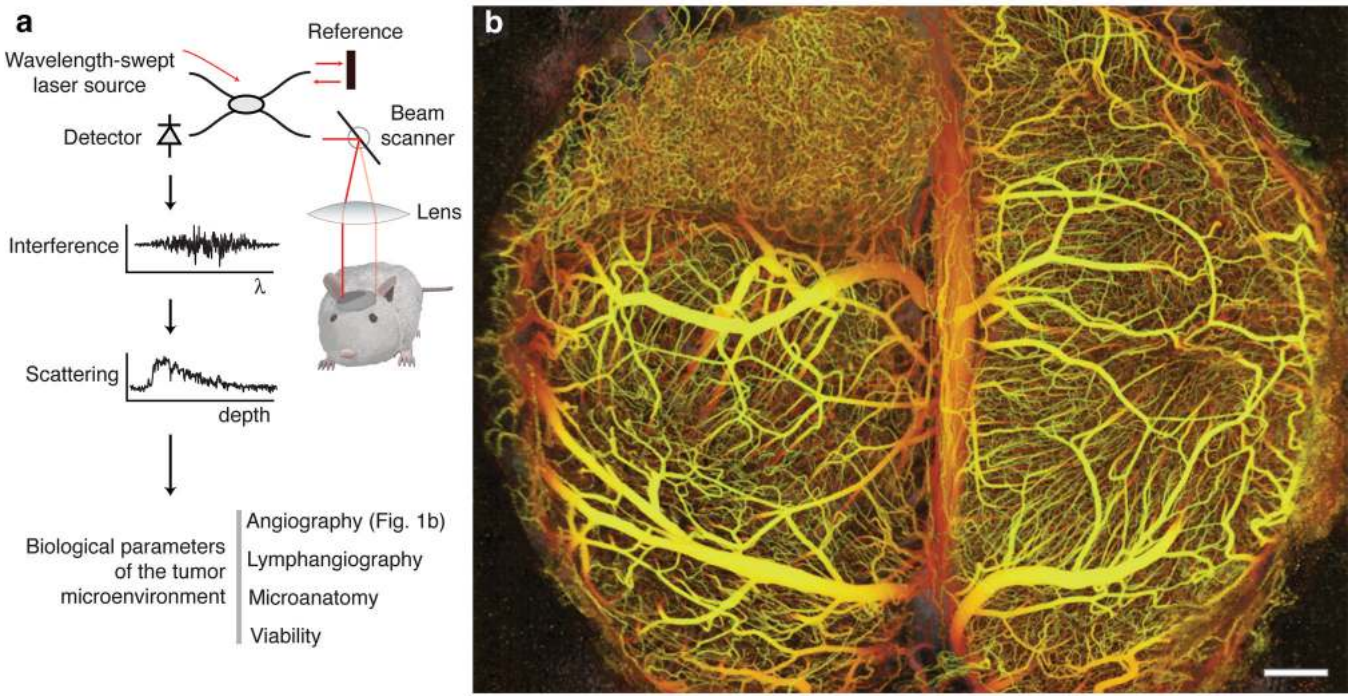

Figure 1.

Principles of *in vivo* multiparametric imaging with optical frequency domain imaging (OFDI). (**a**) An optical beam is focused into the tissue. The light reflected across all depths is combined with a reference beam and the interference signal is recorded as a function of light wavelength from 1,220 nm to 1,360 nm. The amplitude and phase of the reflected light as a function of wavelength is used to localize the reflected signal as a function of depth. At a given depth, the amplitude and phase of the reflected signal as a function of time is used to derive the optical scattering properties and thereby the tissue structure and function.(**b**) The depth-projected vasculature within the first 2 mm of mouse brain bearing a xenotransplanted U87 human glioblastoma multiforme tumor imaged with OFDI. Depth is denoted by color: yellow (superficial) to red (deep). Scale bar, 500 μm.

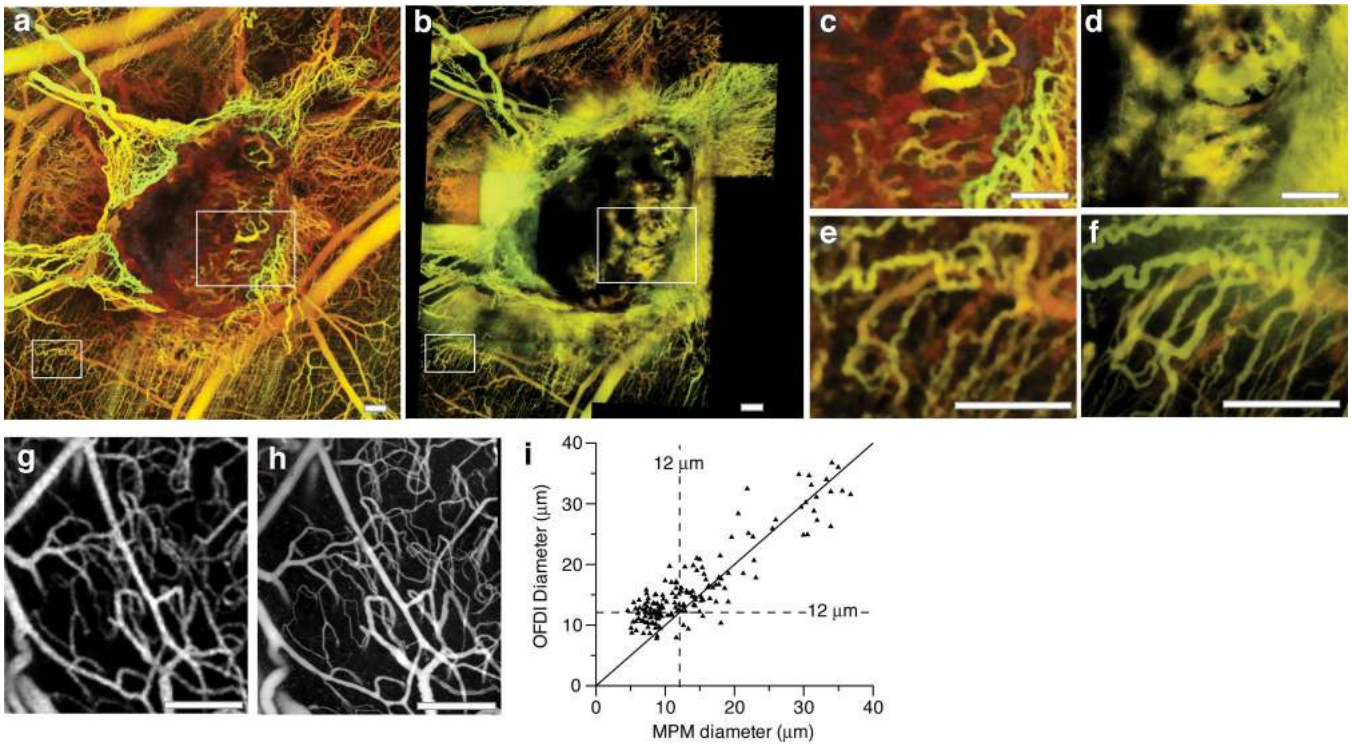

Figure 2.

Comparison of multiphoton and OFDI angiography. (**a**,**b**) Wide-field imaging of an MCaIV tumor implanted in the dorsal skinfold chamber with OFDI (*a*) and MPM (*b*). Imaging with MPM over this field of view required the acquisition and subsequent alignment of 30–40 separate three-dimensional image stacks to sample a field of view equivalent to that of the OFDI instrument. Imaging duration was 10 m for OFDI and 2 h for MPM. Faster MPM imaging times could be obtained using lower magnification lenses at the expense of resolution and depth of penetration. (**c**,**d**) Highlighted regions in *a* and *b* demonstrate the enhanced ability of OFDI (*c*) to visualize deeper vessels and distinguish morphology in regions of vascular leakage relative to MPM (*d*). (**e**,**f**) Differences in resolution of the techniques showing the greater detail of finer vascular structures obtainable by MPM (*f*) in comparison to OFDI (*e*). (**g–i**) The application of automated vascular tracing to registered datasets of normal brain vasculature acquired with OFDI (*g*) and MPM (*h*) allowed quantification of the resolution of OFDI angiography and validation of the morphological measurements obtained from OFDI (*i*). Scale bars, 250 μm.

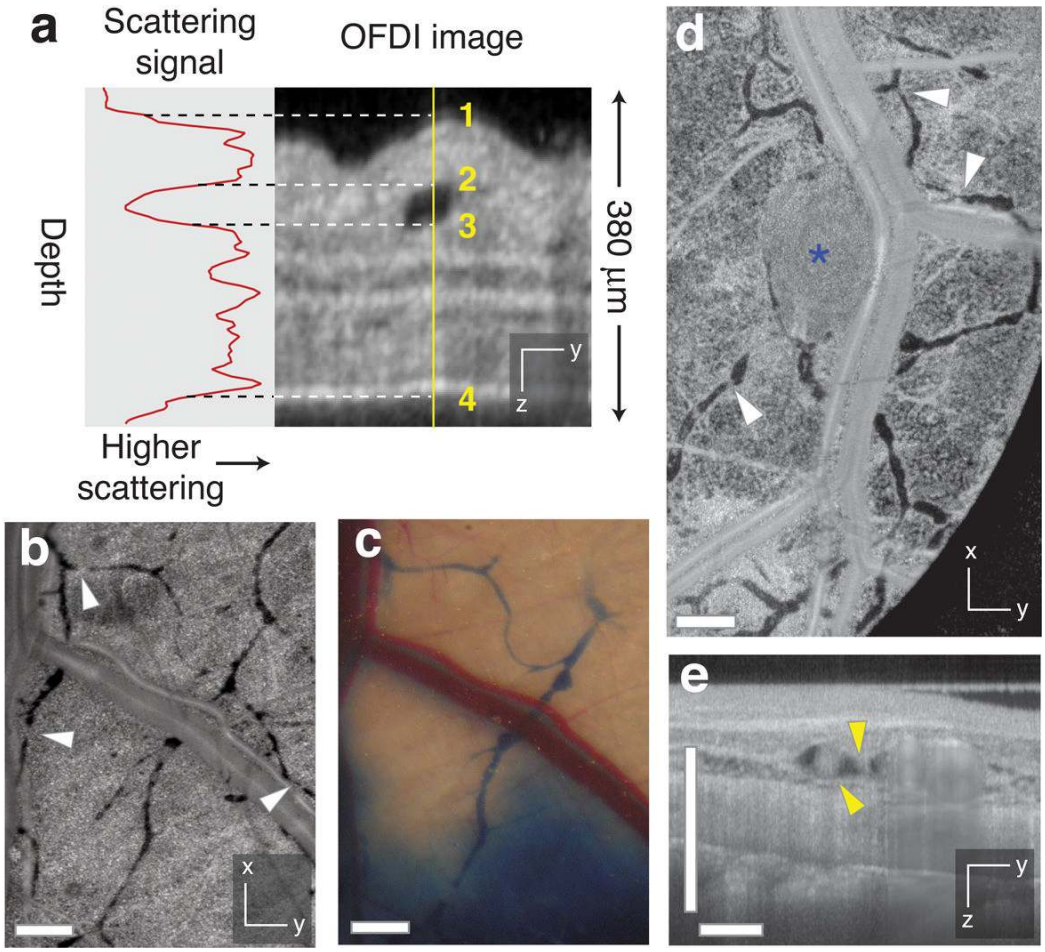

Figure 3.

Contrast-free lymphangiography using OFDI. (**a**) The scattering signal along a single depth scan within an OFDI image of a mouse ear shows the reduced scattering between the upper (2) and lower (3) boundaries of a patent lymphatic vessel. Scattering within the vessel is similar to background levels above the upper surface of the ear (1) or below the lower surface (4). (**b**,**c**) In addition to lymphatic vessels revealed by traditional cutaneous injection of Evan's blue dye (*c*), OFDI was able to detect numerous additional vessels in the normal dorsal skin (*b*) and resolve the lymphatic valves found between individual lymphangions (white arrowhead, ▻). (**d**) HSTS26T tumor (blue asterisk, *) associated lymphatics exhibiting hyperplasia. (**e**) Cross-sectional presentations of a lymphatic vessel showing cellular masses (yellow arrowhead, ►) located near the tumor in *d*. Scale bars, 500 μm.

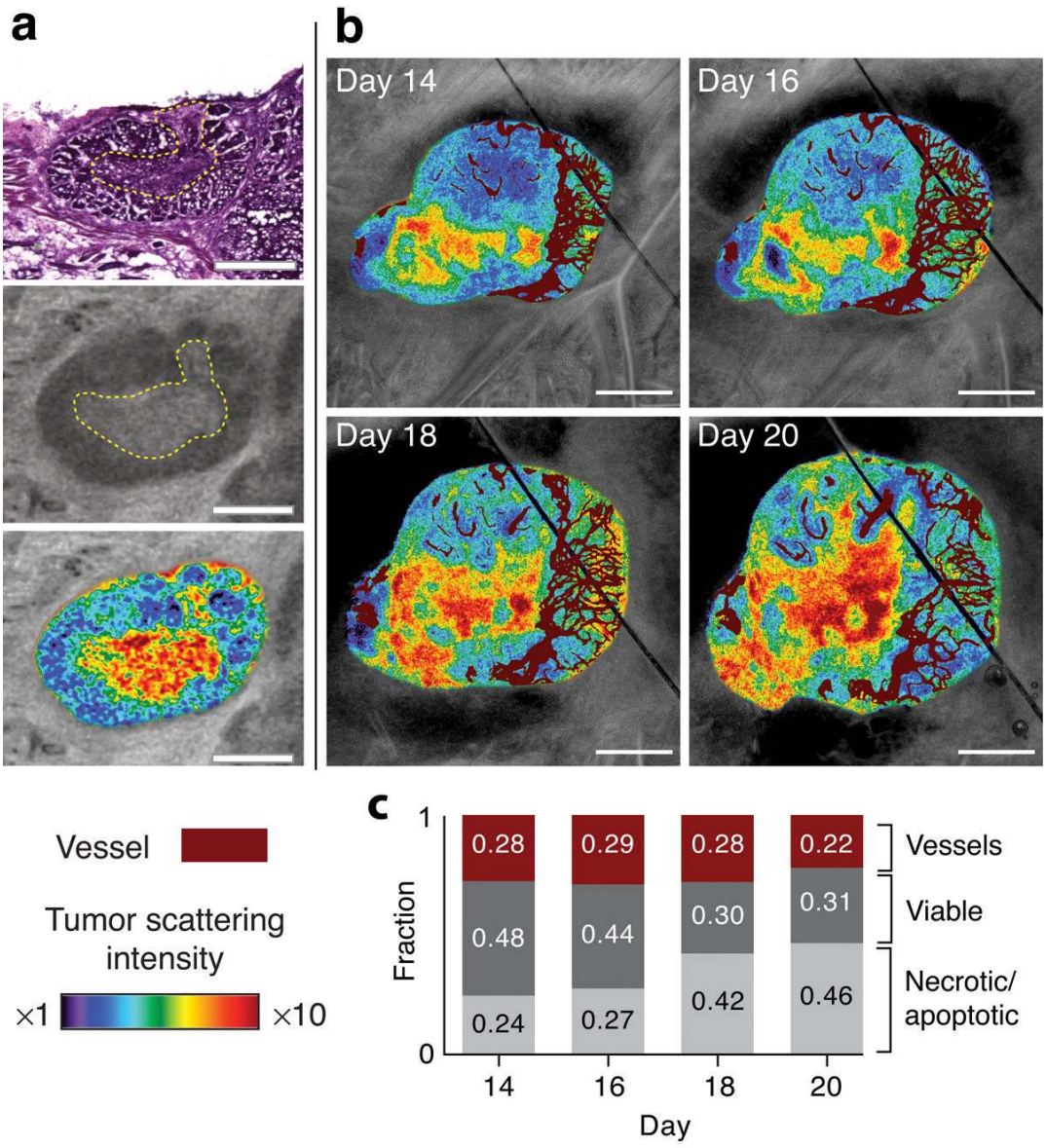

Figure 4.

Imaging tissue viability. (**a**) Comparison of standard hematoxylin and eosin staining (top) with OFDI (middle) reveals association of tissue necrosis with highly scattering regions. Viable and necrotic regions within the same tumor highlighted by color gradients indicating scattering intensity (lower). (**b**) Scattering properties correlated with the microvasculature during tumor progression illustrate the expansion of necrotic/apoptotic regions in areas with minimal vascular supply. (**c**) Quantitative analysis of tissue viability and vascular regions *in vivo* revealed an increase in the fraction of necrotic/apoptotic tissue during tumor progression. Scale bars in **a**, 500 μm; scale bars in **b**, 1.0 mm.

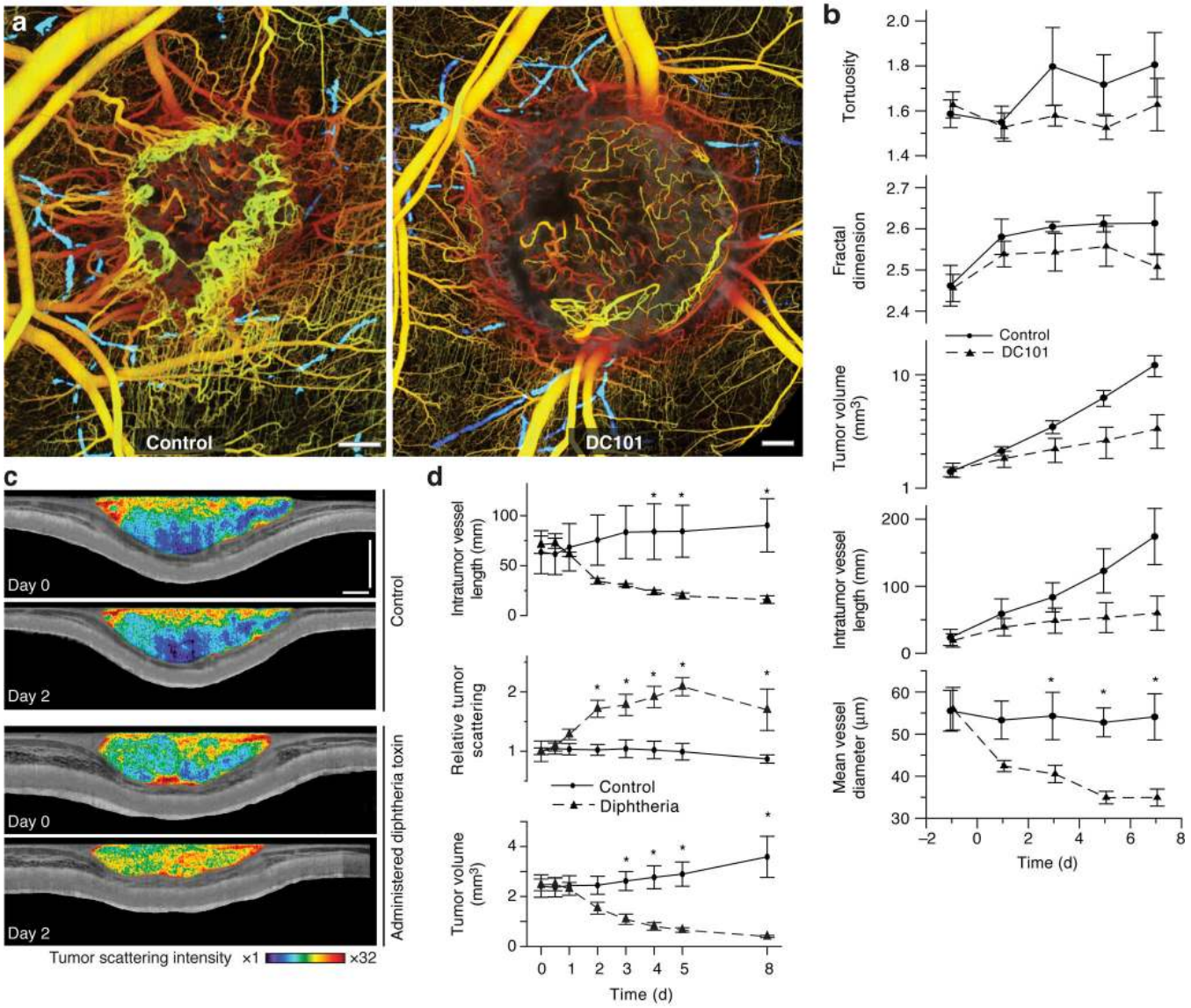

Figure 5.

Multiparametric response of directed anti-cancer therapy characterized by OFDI. (**a**) Representative control and treated tumors 5 d after initiation of anti-angiogenic VEGFR-2 blockade exhibit strikingly different vascular morphologies. The lymphatic vascular networks are also presented (blue) for both tumors. (**b**) Quantification of tumor volume and vascular geometry and morphology in response to VEGF-R2 blockade. Control $n = 5$, Treated $n = 6$. (**c**) Images of tissue scattering immediately prior to and 2d following administration of targeted cytotoxic therapy (diphtheria toxin) or saline to mice bearing human tumor xenografts (LS174T) in dorsal skinfold chambers. Apoptosis induced by diphtheria toxin is manifest as increased tissue scattering relative to control animals. (**d**) Quantification of the response to diphtheria toxin administration. Control $n = 3$, Treated $n = 3$. Scale bars, 500 μm. Statistically significant differences ($P < 0.05$) at given time points are denoted by asterisks.